METABOLIC ENGINEERING 1, 49–62 (1999)
ARTICLE NO. MT980105

Oxygen Consumption Characteristics of Porcine Hepatocytes

Ulysses J. Balis, Kamelia Behnia, Bharath Dwarakanath, and Sangeeta N. Bhatia

Center for Engineering in Medicine and Surgical Services, Massachusetts General Hospital, Harvard Medical School, and Shriners Burns Hospital, Boston, Massachusetts 02114

Susan J. Sullivan

Organogenesis, Inc., Canton, Massachusetts 02114

and

Martin L. Yarmush and Mehmet Toner

Center for Engineering in Medicine and Surgical Services, Massachusetts General Hospital, Harvard Medical School, and Shriners Burns Hospital, Boston, Massachusetts 02114

E-mail: mtoner@sbi.org

Oxygen uptake rate (OUR) of hepatocytes is an important parameter for the design of bioartificial liver assist (BAL) devices. Porcine hepatocytes were cultured in a specially constructed measurement chamber with an incorporated mixing system and a Clark polarographic oxygen electrode. Signal noise associated with conventional Clark electrode implementations was circumvented by the combination of real time digital numerical averaging and subsequent finite impulse response (FIR) spectral filtering. Additional software allowed for the automated generation of cellular oxygen consumption coefficients, namely, V_{max} and $K_{0.5}$, adding a high degree of objectivity to parameter determination. Optimization of the above numerical techniques identified a 0.1 Hz/200 data point sample size and a 0.004 Hz cutoff frequency as ideal parameters. V_{max} values obtained for porcine hepatocytes during the first two weeks of culture showed a maximal consumption of 0.9 nmole/sec/10^6 cells occurring on Day 4 post seeding, and a gradual decrease to 0.31 nmole/sec/10^6 cells by Day 15. $K_{0.5}$ values increased from 2 mm Hg on Day 2 to 8 mm Hg by Day 8, with gradual subsequent decrease to 4 mm Hg by Day 15. The V_{max} and $K_{0.5}$ values measured for porcine cells were higher than maximal values for rat hepatocytes (V_{max}: 0.43 nmole/sec/10^6 cells, $K_{0.5}$: 5.6 mm Hg) and thus may necessitate significantly altered BAL device design conditions to ensure no oxygen limitations. Finally, these results highlight the need for species specific characterization of cellular function for optimal BAL device implementations.

Key Words and Phrases: **Oxygen uptake rate; hepatocytes; bioreactor; bioartificial liver; digital signal processing; porcine.**

INTRODUCTION

The development of technologies needed in the fabrication of functioning bioartificial liver (BAL) support devices has progressed at a steady pace in the last decade. As implementation issues now focus upon the scaling of system size for human support, adequate device biomass has become an important criterion. Correspondingly, cell culture efforts have shifted from rat to larger species, specifically porcine, in an effort to identify a source of hepatocytes which could supply the necessary numbers for human use.

In BAL designs which utilize large numbers of hepatocytes, it is essential that the bioreactor topology insure that no significant portion of the cells is exposed to oxygen tensions below that required for optimal viability and metabolic output. Otherwise, the oxygen consumption could lead to local domains where a significant fraction of cells are either hypometabolic or dead from low oxygen tension (Foy *et al.*, 1994; Gerlach *et al.*, 1990; Hu *et al.*, 1997; Jauregui *et al.*, 1996; McGuire *et al.*, 1995; Nyberg *et al.*, 1992a, 1994, Sielaff *et al.*, 1997; Stefanovich *et al.*, 1996; Yarmush *et al.*, 1992).

This is particularly true of newer high-density cell packing topologies or multicellular systems (Bader *et al.*, 1995; Dixit, 1994; Gerlach, 1996; Gerlach *et al.*, 1994; Hu *et al.*, 1997; Hughes and Williams, 1996). Adjusting physical properties of the bioreactor such as perfusion flow rate, inlet

1096-7176/99 $30.00

oxygen tension, cell density and the actual reactor geometry to assure adequate oxygenation of all cells may optimize cell function, and thus bioreactor performance. Among one of the key parameters in BAL designs is the oxygen uptake rate (OUR) of hepatocytes. Although OUR has been well characterized for rat hepatocytes (Foy *et al*., 1994, Hu *et al*., 1997; Rotem *et al*., 1992; Shatford *et al*., 1996), information has not been previously reported for porcine hepatocytes for their ultimate use in a large-scale BAL system.

In this study, we extended our prior technique of oxygen consumption measurement of anchorage-dependent cells, to accurately assess the OUR characteristics of porcine hepatocytes. The accuracy of oxygen measurement was improved by combining real-time numerical averaging with subsequent spectral filtering to selectively remove noise. OUR results obtained from porcine hepatocytes revealed different metabolic states for immediately postseeding and long-term stable-culture conditions, with the former state exhibiting high $K_{0.5}$ and low V_{max} values and the latter exhibiting the inverse of these conditions. Further, the initial porcine V_{max} values were significantly higher than those previously reported for rat hepatocytes, highlighting the need for species-specific metabolic cell information when designing BAL systems, to insure optimal cell performance.

MATERIALS AND METHODS

Materials

Dulbecco's Modified Eagle Medium (DMEM) with 4.5 g/L glucose, fetal bovine serum (FBS), 10× concentrated phosphate-buffered saline (PBS), penicillin, streptomycin and collagenase were purchased from Gibco (Gaithersburg, MD), hydrocortisone from Upjohn (Kalamazoo, MI), epidermal growth factor (EGF) from Collaborative Research (Bedford, CA), insulin from Squibb (Princeton, NJ). All other chemical were purchased from Sigma (St. Louis, MO). DMEM was utilized for all culture experiments and was supplemented with 10% (v/v) FBS, 200 units/mL penicillin, 200 units/mL streptomycin, 7.5 mg/ml hydrocorticone, 20 ng/mL EGF, 7 mg/mL glucagon, and 0.5 units/mL insulin. The pH of this media when allowed to equilibrate with a 10% CO_2 environment was 7.4. Twenty nM 4-{2-Hydroxyethyl}-1-piperazine-ethane-sulfonic acid (HEPES) was added to the above DMEM to form a 7.3 pH solution when equilibrated with 10% CO_2 gas and a 7.8 pH solution when equilibrated with ambient air. Gas mixtures were obtained from Northeast Airgas (Manchester, NH), and gas compositions were certified to an accuracy of at least 0.05 mm Hg. Ultrapure nitrogen for oxygen exclusion jacketing was certified to be 99.998% pure (Grade 4.8; 20 ppm total impurities, 5 ppm oxygen, 1 ppm hydrocarbons, and 3 ppm water).

Hepatocyte Isolation and Culture

Porcine hepatocytes were obtained from Organogenesis, Inc. (Canton, MA) and consisted of hepatocytes isolated from 8.3 ± 3.0 kg ($n = 30$) Yorkshire/Hampshire hybrid pigs (Parsons, Inc., Hadley, MA). Briefly, pigs were systemically anesthetized and heparinized, and the exposed liver cannulated. Three to four liters of cold (4 °C) Ringers Lactated Buffer (RLB) was infused at a rate of 300 mL/min. This was followed by 37 °C 0.2% EDTA infusion of approximately 1 liter followed by perfusion with pH 7.4 buffered collagenase at a flow rate of 150–200 mL/min. Following enzymatic digestion, the tissue was sequentially processed through 200- and 100-μm stainless steel sieves and washed in cold medium. Typically, between 3.0×10^9 and 1.4×10^{10} cells were obtained (mean $= 6.7 \times 10^9$) with viabilities ranging from 65 to 90% (average: 85%), as determined by trypan blue staining. The purity of the initial cell population was >95% hepatocytes as assessed by in situ albumin staining. Porcine hepatocytes were cultured in P60 tissue culture dishes (Falcon, Lincoln Park, NJ) coated with Type I collagen, using a procedure modified from Elsdale and Bard (1972) as described previously (Dunn *et al*., 1991). Following 30 min incubation at 37 °C, the P60 dishes were washed twice with DMEM. Porcine hepatocytes were subsequently seeded on the precoated dishes with 4 ml of a 0.25×10^6 cell/ml suspension, for a total initial seeding density of 1×10^6 cells/dish. Cultures were then incubated at 37 °C with a 10% CO_2 environment and allowed to stabilize for 24 h prior to commencement of OUR experiments.

Rat hepatocytes were isolated from 2 to 3 month-old Lewis rats (Charles River, MA) as described in detail elsewhere (Dunn *et al*., 1991). Briefly, 200-400 million cells were obtained from a single isolation, with viabilities >90%, as determined by trypan blue staining. Both collagen coating and culture preparations were carried out similarly to the methods used with porcine hepatocytes as described above.

OUR Measurement Device Description

The device used to perform OUR measurements consisted of a laithed polycarbonate insert, which formed an interference-fit seal with the top rim of a P60 tissue culture dish (Fig. 1) as previously described (Foy *et al*., 1994). When inserted upon a P60 dish, the resulting enclosed volume was 11.5 ml. A polarographic oxygen electrode (Diamond-General, #731 MiniClark PO_2, Ann Arbor, MI) was incorporated into this insert, as was a gear-reduction motor and internal magnet assembly, which propelled a magnetic stir bar within the culture dish chamber. This device differed from our earlier design (Foy *et al*., (1994) in that the fluid outlet hole was omitted, to minimize the possibility of air bubbles entering into the chamber.

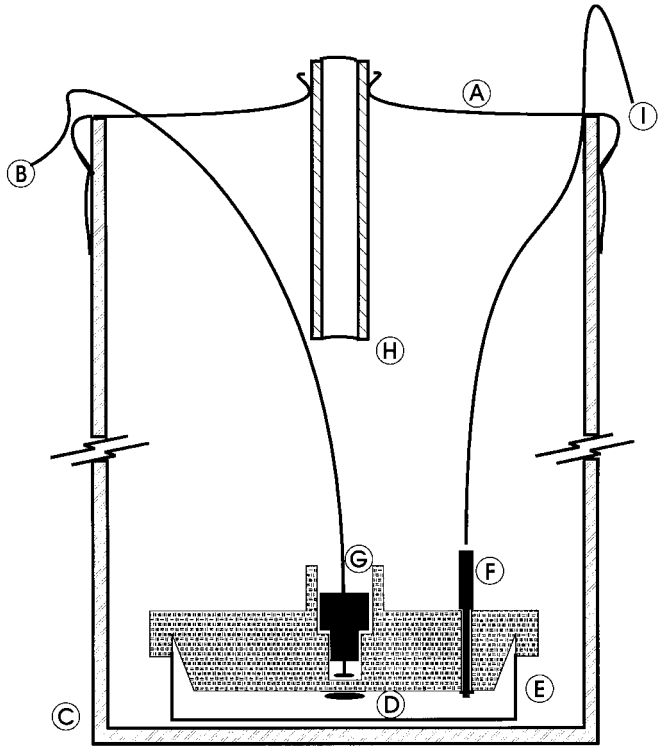

FIG. 1. Schematic diagram of our measuring device and protective nitrogen jacketing: (A) aluminum foil wrapping to minimize intrusion of external oxygen into nitrogen-jacketed volume, (B) electrical connection for stir bar motor, (C) 2000 mL glass beaker, (D) Teflon-coated magnetic stir bar within chamber, (E) P60 tissue culture dish containing attached hepatocytes, (G) Clark miniature polarographic oxygen electrode, (G) stir bar motor, (H) nitrogen inlet tube, (I) shielded electrode cable linked to dedicated signal conditioner/amplifier.

During assembly, the P60 dish was filled with 15 ml of HEPES medium, which had been previously bubbled for 30 seconds with a 10% CO_2, 20.9% O_2, and a balance N_2 air mixture, to form a buffered pH of 7.38. The device was subsequently lowered on the P60 dish at a slight angle, allowing for all bubbles to escape. This process was facilitated by the use of a 23 gauge hypodermic needle, employed as a bubble lance. Prior to insertion, the bottom surface of the device was premoistened with medium to minimize the formation of bubbles near the stir bar, Clark electrode, or dish rim. Following the device's final pressing into the P60 dish, a visual inspection was conducted to insure that no bubbles were entrapped within the 11.5-ml volume. If bubbles were identified, the assembly process was repeated. This step was taken to minimize potential artifacts caused by oxygen at low internal oxygen tensions. Thereafter, the device was placed in an outer container which was continuously purged with 100% high-purity nitrogen throughout the duration of the experiment. All experiments were carried out in a warm room (37 °C, 50% relative humidity) with conditions verified prior to and after each run, as polarographic oxygen electrode calibration is dependent upon stable temperature. Finally, ingress/egress to the warm room was minimized through the air-tight door, to minimize transient pressure changes which could also potentially affect the calibration of the Clark electrode. All experiment supplies such as compressed gasses and media were allowed to temperature equilibrate for at least 30 min prior to their use.

Transconductance current from the polarographic oxygen electrode was linked to a dedicated amplifier (Diamond Electro-Tech, Chemical Microsensor Amplifier #1201, Ann Arbor, MI) via a double-shielded small signal coaxial cable with SMC connectors, to minimize electrical noise. A resulting milivolt signal, linearly proportional to the measured oxygen tension, was sent to a high performance 16 bit analog-to digital converter (ADC) (DAS1600-16L, ComputerBoards, New Bedford, MA) incorporated into an 80486 66 – MHz pc-compatible system, running the Windows 3.11 (Microsoft, Redmond, WA) and Norton Desktop 3.0 (Symantec, Redmond, WA) operating systems. Acquisition software was developed utilizing Visual Basic 3.0 (Microsoft, Redmond, WA) as the graphical interface, with embedded sections of C and assembly language code as needed for speed optimizations.

OUR Measurement Technique

On-line numerical techniques. An overall data flow chart of on-line data processing methods is depicted in Fig. 2. Briefly, for all the experiments, on-line noise reduction (Fig. 2A) consisted of linking a polarographic Clark oxygen electrode to a instrumentation-grade amplifier, which allowed for precise membrane bias, gain and zero offset calibration. The resulting voltage signal was sampled at 20 Hz in 10 s intervals, by a 16 bit analog-to-digital converter (ADC), with the resulting 200 data points contributing toward; a software-averaged real-time value. The voltage range setting of the ADC signal input was matched to the full scale range of the electrode amplifier (1 V), in order to maximize its 16 bit utilization. This provided for approximately 96 dB of dynamic range, which was further enhanced by 10 dB, through the use of signal averaging. On-line averaged data was plotted on the computer display, and concurrently stored in 10 s intervals. The off-line data storage format consisted of parametric time-value pairs, with time values in 0.1 s center-weighted resolution and oxygen tension in 0.001-Torr resolution. Short time-scale noise was effectively removed with this method. For acquisitions performed for electrode calibration and linearity characterization, the above conditions were modified to use a 20-s interval to increase the number of data points to 400, with a concomitant increase in signal averaging precision from 10 to 14 dB.

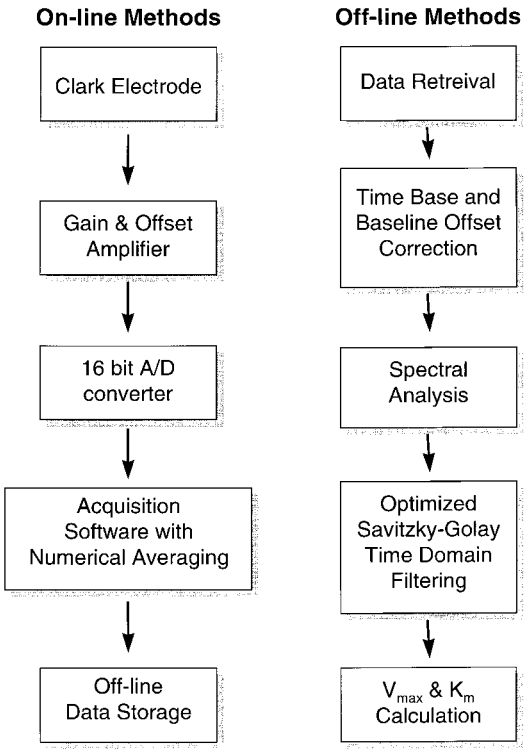

FIG. 2. Block diagram of major components of on-line and off-line signal processing incorporating (A) on-line and (B) off-line functionality. On-line methods encompass analog signal conditioning and analog to digital conversion combined with real-time numerical signal averaging. Following data storage and subsequent retrieval, off-line methods encompass normalization of data and subsequent spectral analysis and filtering to remove Clark electrode noise. V_{max} and $K_{0.5}$ are numerically derived from resulting data sets.

Off-line numerical techniques. Oxygen tension vs time parametric data as measured upon on-line processing described above was processed off-line to generate OUR vs oxygen tension curves. The software packages and numerical tools used for off-line processing of data included: Excel 7.0 and Visual Basic 3.0 (Microsoft Corporation, Redmond, WA), Mathematica 3.0 (Wolfram Research, Champaign, IL), DADiSP (DSP Development Corpt., Cambridge, MA), Statistica 4.5 (Statsoft Corporation, Tulsa, OK) and SigmaPlot 3.0 (Jandel Corporation, San Rafael, CA). Figure 2B provides an overview of the steps involved in processing the off-line data. Briefly, the stored parametric data was zero-normalized to endpoint calibration oxygen tensions, to correct for minute baseline offset encountered following initial pre-experiment calibration. An equidistant time-base normalization (via second order polynomial interpolation) was performed on the resulting data, to correct for slight interval variations in the parametric time data intervals. This allowed for the generation of one-dimensional vectorized (implicit-time) data sets suitable for use with subsequent spectral analysis packages. Subsequently, DADiSP was used to characterize the Clark electrode's frequency noise. This allowed for optimal noise reduction. To accomplish this, Savitzky–Golay time domain filtering was applied to normalized data. As a result, OUR vs $[O_2]$ curves were generated and V_{max} and $K_{0.5}$ parameters values were computationally generated.

Spectral characterization. To accomplish spectral analysis, an initial fast Fourier Transform (FFT) was applied to off-line normalized time-tension data [34]. Intermediate time-scale noise and resulting data was displayed in power spectrum format, allowing for the identification of electrode noise and actual signal passband regions within the overall spectral range of 0.00001 to 0.1 Hz. With the identification of a sizable bandwidth between these two different spectral regions, it was possible to specify a cutoff frequency which would exclude the majority of Clark electrode noise, without compromising OUR data. A Savitzky–Golay (SG) finite impulse response (FIR) filter was used to carry out frequency-domain filtering in the time domain, to reduce computation complexity (Press *et al.*, 1992a). The cutoff frequency initially identified via spectral methods was mapped to a ninth-order SG filter (actually performed with a numerically equivalent 912th-order discrete Remez Exchange filter used within DADiSP) and all OUR data was subsequently processed utilizing this FIR transform.

The resulting data set was then utilized to generate OUR vs oxygen tension plots. Resulting data were fitted to Michaelis–Menton kinetics defined as follows

$$\frac{dP}{dt} = \frac{(-(V_{max}P)/(K_{0.5}+P))}{(N_c/kD)}$$

where t is time (s), P is the oxygen partial pressure within the enclosed device (mm Hg), D is the device total liquid volume displacement (11.5 mL), N_c is the number of cells in the device, and k is the conversion factor between oxygen partial pressure to oxygen concentration for saline media (1.19 nmol/mL-mm Hg) (Foy *et al.*, 1994). To generate the slope information, the derivative was obtained by generating a local-domain least-square fit for every data point. Thus, computation of the OUR was carried out by utilizing a sliding-window 60 s linear regression. The V_{max} was calculated by averaging all OUR rates above 20 mm Hg PO_2, as this tension range was noted to globally fall outside the zone of $K_{0.5}$ diminution. $K_{0.5}$ was calculated by obtaining the oxygen tension at 50% V_{max} from the OUR vs tension plot.

Device setup and calibration. Device characterization, calibration, and measurement on cells were all carried out in

the warm room (37 °C). Polarographic electrodes were prepared pursuant to the manufacturer's recommended protocol. Briefly, the electrode tip was cleaned in ethanol, and then dipped into a solution of saturated potasium chloride for 30 s under 25 mA current to precharge the platinum/silver complex with chloride. Subsequently, a 25-μm thickness polyethylene membrane was placed over the KCL-soaked tip and secured with an O-ring. Excess polyethylene proximal to the O-ring was removed with a razor blade, as excess membrane could become a bubble trap near the electrode tip. Offset current and noise within the electrode was elevated for between 1 and 5 h following membrane replacement, making it necessary to allow for a 5 h minimum post-replacement equilibration period. Electrode stability was subsequently verified by its placement in HEPES media which was bubbled with a 21% oxygen gas mixture (159 mm Hg PO_2), with the stir bar spinning at a nominal rate of 1800 rpm. Zero set-point validation was then performed by placing the electrode in a 100% nitrogen environment. All oxygen tension measurements were acquired with the electrode electrically biased at the manufacturer's recommended value of -750 mV.

Prior to OUR experiments, the electrode was calibrated at 159 and 0 mm Hg PO_2, in a similar manner as described above. The OUR chamber was then assembled 5 min prior to OUR measurements, and data collection was initiated. Data collection was terminated when the oxygen tension of the closed system reached the calibration zero setpoint, indicating complete consumption of oxygen within the 11.5 ml volume. Following data collection, the electrode was recalibrated at 159 mm Hg PO_2 to identify drift, if present. In all experiments, the electrode drift was less than 1.5%. During all experiments, adequate mixing of the chamber was implemented by utilizing the identical mixing speed of 1800 rpm as that previously described by Foy *et al.* (1994).

Long-term stability of the electrode was assessed by filling a P60 dish with media prebubbled with a 21% oxygen balance nitrogen mixture. The device was assembled in the usual manner and placed in the continuous nitrogen shroud. Oxygen tension was recorded for 2 h using the nominal fluid mixing, data sampling, and numerical averaging experimental parameters.

Data-flow. A custom display interface and data management program was constructed in Visual Basic. Within this program, the raw data was loaded in its entirety and displayed, allowing for user selection of several regions of interest, which guided further data analysis. Using the initial and final calibration set points within the data, this program utilized a user-selected data segment as a zero reference. The average of the oxygen tension over this interval was applied to the entire data set to formally normalize the data to a calibrated zero oxygen tension. This was followed by SG filtering and automated OUR vs oxygen tension plot generation, along with automated calculation of V_{max} and $K_{0,5}$ values. This program finally generated export files of the zero-corrected data and SG-filtered OUR plots for further statistical analysis.

Artifact Quantitation

Device characterization. Accurate measurement of V_{max} and $K_{0.5}$ parameters depends on minimization of oxygen leakage into the closed system, insuring that the liquid within the chamber is well mixed, and the maintenance of constant temperature and pressure. To address the first issue, the device was placed in a 2000 mL beaker and sealed with Parafilm and aluminum foil. This shroud was then continuously purged with 100% nitrogen gas during both experiment and calibration runs. The oxygen leakage rate under low tension conditions was measured by allowing a sample hepatocyte culture to consume oxygen to 0.0 mm Hg, using standard experimental protocols as already described. Nitrogen purging of the outer shroud was continued from this point and measurement of the internal oxygen tension was continued.

Clark electrode characterization and quantitation. To characterize the performance of the miniature electrodes utilized within the chamber, a large-scale standard curve calibration was generated by initially sealing the electrode in a 100% N_2 chamber of 2 L displacement, maintained at 100% relative humidity to prevent electrode desiccation. Incremental 5-cm^3 volumes of USP grade 100% oxygen were subsequently injected at 5-min intervals. A similar small-scale standard curve was constructed by conducting the above experiment with 1-cm^3 serial injections. During these runs, the acquisition software was programmed to utilize 400 samples for each 20-s data point. After each injection, the system was allowed to equilibrate for 5 min before measurement. Subsequently, five more minutes were allowed to pass before the next injection, to allow for visual confirmation that the oxygen tension had indeed stabilized. Final calibration values were obtained by numerically averaging the values obtained from the final 2 min of each period, by which time the oxygen tension had fully plateaued.

DNA collection and measurement. Following OUR measurement, the hepatocytes were harvested and stored for subsequent DNA quantification. Briefly, the supernatant media and any suspended cell products were removed and the cells harvested by scraping the surface, followed by a phosphate-buffered saline rinse, in triplicate. The resulting suspension was centrifuged for 5 min at 1200 g, and the

pellet resuspended in 20 ml of PBS. Samples were subsequently stored at −80 °C until DNA analysis. DNA quantification was performed by methods previously described (Steen *et al.*, 1993). Samples were thawed and aliquoted in quadruplicate into a standard flat-bottom 96-well microtitre plate, along with DNA standards between 0 and 100 μg/ml. Hoechtst 33342 DNA stain (Molecular Probes, Eugene, OR) was added and the plate was allowed to incubate at 24 °C for 30 min. The plate was subsequently read with a fluorescence plate reader (Molecular Devices, San Luis Capistrano, CA) with excitation and emission frequencies of 290 and 361 nm, respectively. Standards were plotted on a linear scale and assessed by conventional linear regression methods.

Statistical analysis. Error reported in the text are reported as standard deviation of the mean. Data are presented from three porcine and three rat hepatocyte isolations. Experiments were generally repeated four times per measurement day per isolation, for a total of approximately 60 porcine experiments and 20 rat experiments. Assessment of the statistical significance of difference in means was determined by the application of both single and multiple analysis of variance (ANOVA), where appropriate, with calculations performed within the Statistica software package.

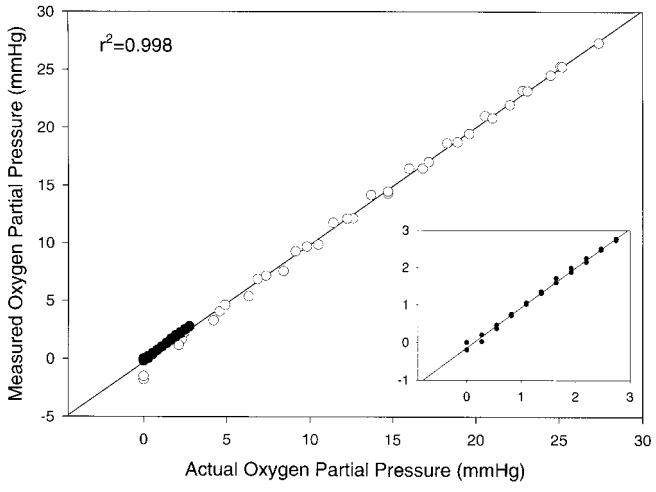

FIG. 3. Measured oxygen partial pressure vs. actual oxygen partial pressure to determine the linearity of the Clark polarographic oxygen electrode. Open circles and filled circles represent 1.5% and 0.1% PO_2 oxygen tension increments, respectively. Three calibration runs are superimposed for each range. The lines on each graph are linear regression fits to the collective data. The inset depicts an expanded view of the small scale range, demonstrating retained linearity for oxygen tensions between 0 and 3 mm Hg.

RESULTS

Device Characterization

To verify that the OUR apparatus neither allowed the inflow or outflow of oxygen during experimental runs, several calibration procedures were devised to test the integrity of the overall system. To characterize oxygen egress from the system, medium which was initially set to 159 mm Hg PO_2 was placed in the chamber, while its immediate exterior was jacketed with high-purity nitrogen gas (<0.05 mm Hg PO_2) for 6 h, The rate of leakage was obtained by dividing the change in oxygen tension within the chamber by the total experiment time in seconds. Following an initial 10 to 20 min period of system stabilization, leakage rates were consistently less than 5.5×10^{-4} mm Hg/s, which was outside the time-scale of typical OUR experiments in this study. The leak likely originated from imperfections in the interference fit between the OUR device and the rim of the P60 tissue culture dish. To characterize oxygen leakage into the system during low chamber tensions, a typical porcine hepatocyte OUR experiment was continued after reaching 0.0 mm Hg PO_2 tension. Oxygen tension remained at 0.0 mm Hg PO_2 as long as nitrogen jacketing was left in place. As a final measure, demonstrating the necessity for continuous nitrogen flow and the responsiveness of our measurement system, the nitrogen jacket was opened to the ambient environment, at which time oxygen tension increased at a rate of 1×10^{-3} mm Hg/s.

It is well established that polarographic oxygen electrodes consume a small but measurable quantity of oxygen in the process of oxygen tension measurement, with manufacturer's specification for our device indicating an oxygen consumption of 0.936 nmole/h. For the chamber volume of 11.5 ml utilized within this study, with a known oxygen solubility constant of 1.19 nmol/mL/mm Hg, this corresponded to an oxygen consumption rate of 6.8×10^{-2} mm Hg/h, which was far slower than the OUR rates measured in this study, and subsequently inconsequential to the overall assessment of oxygen leakage. Therefore, OUR measurements obtained in this study were representative of the actual cellular consumption rate, with minimal distortion from either electrode oxygen consumption or chamber leakage.

FIG. 4. Efficacy of numerical signal averaging for reducing broadband spectral noise. The left histograms represent Clark electrode noise frequency spectra encountered with different numerical averaging conditions and the right plots depict the rendered OUR curve for each respective condition set with: (A, E) 1.0 Hz periodicity and $n = 20$ averaging size, (B, F) 0.5 Hz and $n = 40$, (C, G) 0.2 Hz and $n = 100$, and (D, H) 0.1 Hz and $n = 200$. As sample size increases from (A) through (D), improvement in OUR plot quality is observed. However, even with a sample size of $n = 200$ (H), significant noise artifact remains within the OUR curve, necessitating further filtering.

METABOLIC ENGINEERING **1**, 49–62 (1999)
ARTICLE NO. MT980105

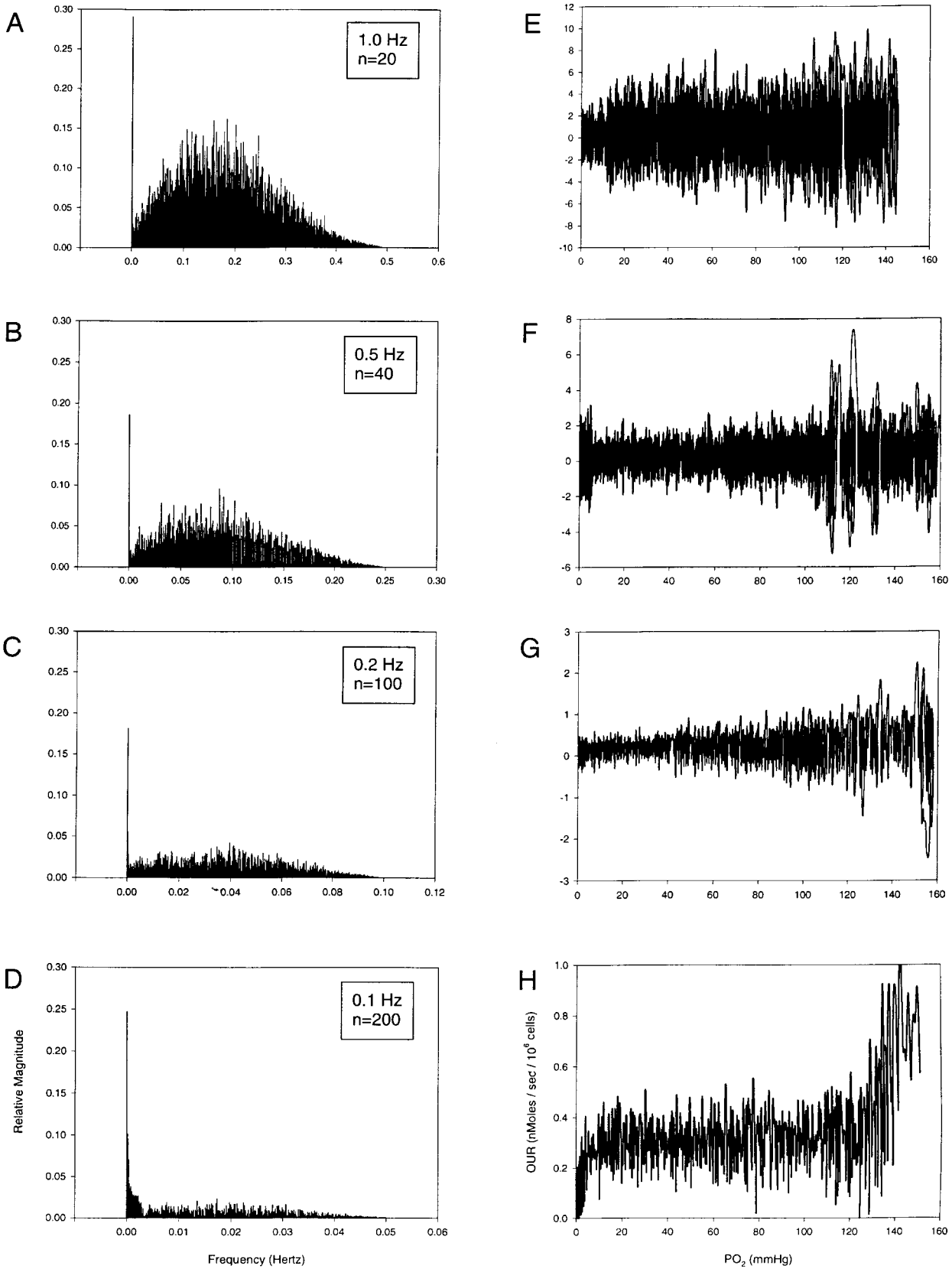

Electrode Characterization

To assess response time of Clark electrodes used in our study, electrodes were sequentially exposed to 21 and 0% oxygen atmospheres, and were shown to equilibrate to 0.1% of the final target tension within 20 s, rendering a time constant of approximately 5 s. As signal numerical averaging was performed over either 10- or 20-s intervals during OUR measurements, artifacts arising from electrode response time was therefore excluded.

Clark electrodes have been criticized in the literature for their potentially nonlinear response in the 0 to 10 mm Hg PO_2 range (Starlinger and Lubbers, 1972; Vanderkooi *et al.*, 1991). To verify the linearity of polarographic electrodes at low and full-scale oxygen tensions, a special experimental format was devised to allow for precise measurement of steady-state electrode response under low tension conditions. Initially, full-scale linearity measurements were carried out using DMEM equilibrated to 159 mm Hg PO_2, followed by electrode introduction into a 100% nitrogen. This two-point calibration was repeated ten times, with resulting values exhibiting a standard deviation of 0.10 and 0.22 mm Hg for low and high tension measurements, respectively. To assess electrode performance at low oxygen tensions, measurements were obtained from the stepwise injection of known uniform quantities of USP grade 100% oxygen into ultrapure nitrogen. Preliminary attempts to conduct this calibration without an outer nitrogen jacket proved impossible, due to quiescent oxygen leakage into the system. Consequently, this system was thoroughly jacketed with an actively purged outer nitrogen environment, as already described. For both small (0 to 3 mm Hg) and large scale (0 to 30 mm Hg) ranges, the electrode response was linear with a collective correlation coefficient of 0.998 (Fig. 3), with each range repeated in triplicate. Correlation coefficients for the individual large-scale and small-scale runs were all better than 0.990 and overlapped with high fidelity to the ideal 1: 1 identity slope. Likewise, superimposition of both ranges demonstrated a high degree of fidelity to the predicted slope. For all O_2 tension calculations, partial pressures were corrected for relative humidity.

Numerical Signal Averaging

Spectral techniques for signal processing offer several significant advantages over conventional time-series filtering (Krantz, 1991). Most significant of these is the time-invariance of the spectral approach; modifications performed upon data in spectral format are inherently uniform in their time-series mapping. Additionally, spectral analysis allowed for quantitative assessment of the noise component of the electrode signal, and allowed for tailored removal of noise without time-response damping in the areas of greatest OUR change. Initial work with the miniature polarographic electrodes indicated that they generated significant low frequency noise variation associated with mixed-fluid conditions, which could potentially interfere with the accurate assessment of changes in oxygen tension, particularly in the region of the $K_{0.5}$ transition area. As the $K_{0.5}$ transition periods typically seen in OUR experiments were no greater than 600 s in length, signal averaging for periods of up to one tenth of this interval could be safely justified. Subsequently, these resulting data sets would still accurately trace the actual $K_{0.5}$ curvature, but with greatly attenuated noise. To identify the optimal parameters for real-time signal averaging, Fourier transform-derived frequency spectra were obtained from OUR runs conducted with different sampling intervals and averaging population sizes. Within these spectra, the depicted frequencies spanned 0 Hz to a maximum of one-half of the sampling rate, as stipulated by Nyquist-limit sampling theory (Krantz, 1991).

The spectra depicted in Fig. 4A–4D demonstrate the efficacy of numerical signal averaging for reducing broadband spectral noise. Noise amplitude progressively decreased with increasing averaging sample size. The 1 Hz ($n = 20$) sample rate exhibited the highest amplitude noise while the 0.1 Hz ($n = 200$) sample rate exhibited the least noise. In addition to increasing the averaging number, decreasing the sampling rate had the added advantage of lowering the maximum noise frequency to the Nyquist limit (one-half of the sample rate). The large left peak common to all spectra represents the low frequency information of the $K_{0.5}$ inflection area. All spectral information right of this low frequency peak represents undesirable noise.

The corresponding OUR plots (Figs. 4E–4H) exhibited improved rejection of high-frequency noise with increased averaging number, respectively. For averaging numbers of 20, 40, or 100, the OUR profile was essentially obscured by noise, while the 0.1 Hz ($n = 200$) acquisition series demonstrates a typical, albeit noisy, OUR curve. From this observation, the 0.1 Hz sample rate was chosen for subsequent OUR experimentation, as extended averaging experiments (data not shown) yielded no additional spectral noise reduction (sample sizes of 400, 800, and 1600 were attempted), and could potentially compromise the accurate assessment of $K_{0.5}$ values, due to decreased response rates associated with greater averaging intervals. Although the 0.1 Hz OUR plot exhibited the best noise immunity of the set, it clearly contained residual noise, which was evident in its respective spectrum (Fig. 4H). Close examination of this spectrum reveals a clearband starting at 0.004 Hz. Review of the spectra of our other OUR pilot experiments revealed a similar clearband between the 0.004 and 0.008 Hz range. This provided for a consistent low-pass cutoff frequency, where only noise and not data, could be expected to be removed from spectral filtering, as described below.

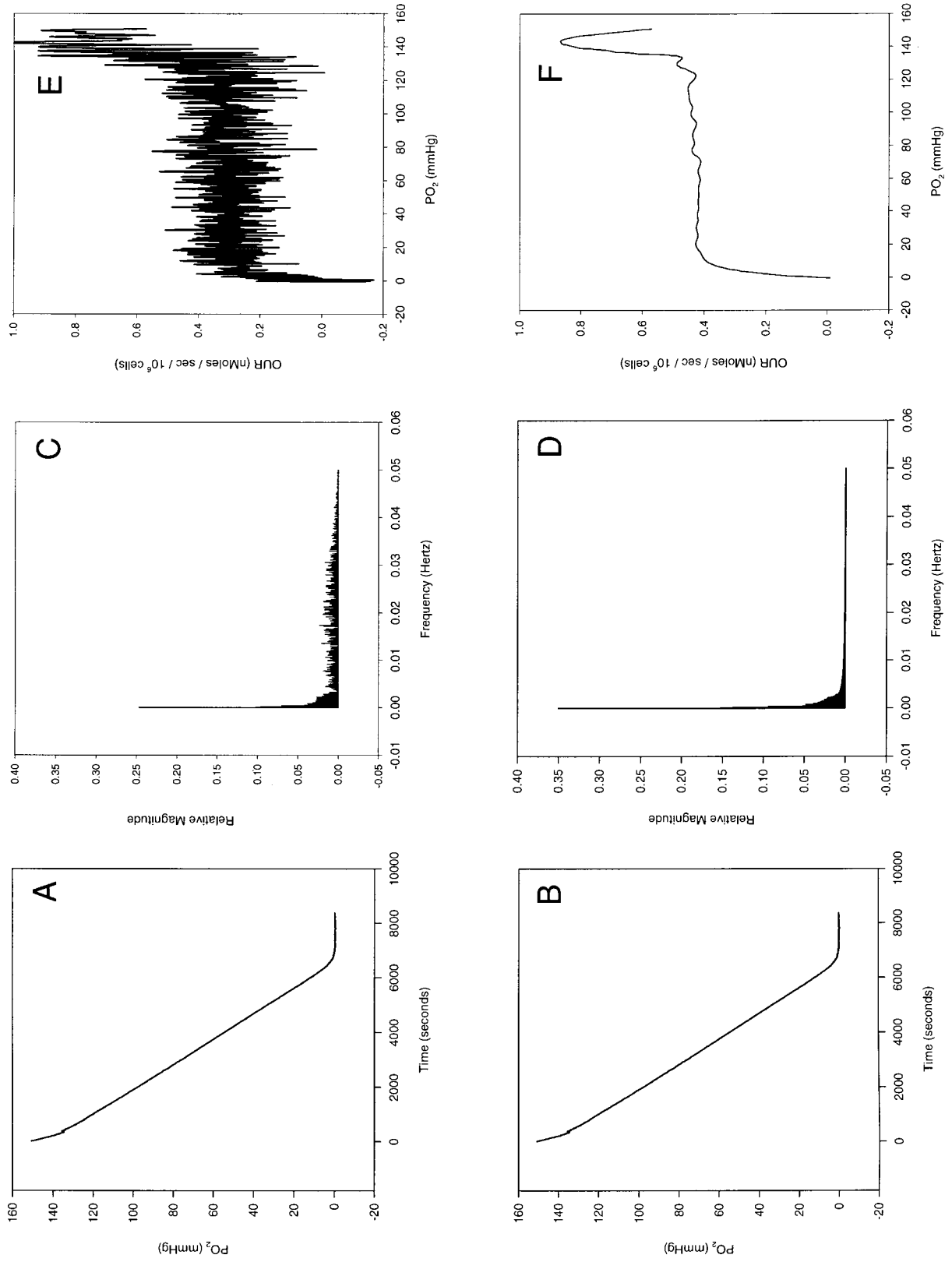

FIG. 5. Demonstration of spectral filtering for removal of residual Clark electrode noise: (A, B) Representative oxygen tension-time data, (C, D) Fourier transform derived power spectra of this data, and (E, F) resulting OUR data based on curve generation from spectral inversion. The second row (B, D, F) is the same experimental data as displayed above, but following optimized spectral filtering where all frequency noise above 0.004 Hz has been selective attenuated (D), resulting in final optimal OUR data (F).

Noise Spectrum Characterization

The above observations of remaining residual noise in the spectral and OUR plots, and the presence of a consistent spectral clearband at 0.004 Hz were all incentives for utilizing digital signal processing (DSP) techniques to further reduce the out-of-band noise, without changing the in-band data of interest. This approach was selected because of the ease with which DSP methods can selectively modulate spectral bands. Consequently, DSP methods allowed for the removal of remaining electrode noise in the out-band region, without compromising the frequency response rate of data measured near the $K_{0.5}$ transition, as would be encountered with conventional low-pass data filtering.

Based on the spectral observations made during numerical averaging optimizations, essentially all of the desired frequency components associated with the V_{max} slope and $K_{0.5}$ transition occurred at frequencies lower than 0.004 Hz. Accordingly, the frequencies of 0.004 and 0.008 Hz were selected as the band-start and band-stop points, respectively, for a 912th order Remez-Exchange SG-FIR filter. Figure 5 depicts the outcome of this DSP technique on a typical data set. Figures 5A, 5C, and 5E depicts the pre-DSP tension-time plot, frequency spectrum, and OUR curves, respectively. Following SG-FIR filtering, Figs. 5B, 5D, and 5F depict resulting data sets. Of greatest importance was the observation that the high-frequency noise was significantly attenuated in the OUR plot, without adversely affecting the $K_{0.5}$ inflection response rate, as was previously noted with excessive conventional low-pass filtering. The resultant plot clearly demonstrates a stable plateau, and a sharp $K_{0.5}$ transition region. The clarity of these OUR curves, following numerical processing, was evident in all runs of this study. The corresponding spectrum of DSP-processed data shows the desired outcome, manifest as an extremely sharp cutoff frequency of 0.004 Hz with preservation of all the low frequency information to the left of this cutoff. As predicted by the use of a 912th order FIR, the noise floor in frequencies greater than the stop-band was less than 70-dB below that of the pass-band signal level.

The consequences of this type of signal processing are far more evident on the corresponding OUR plot, than on the initial oxygen tension data, as the derivative is a mathematical

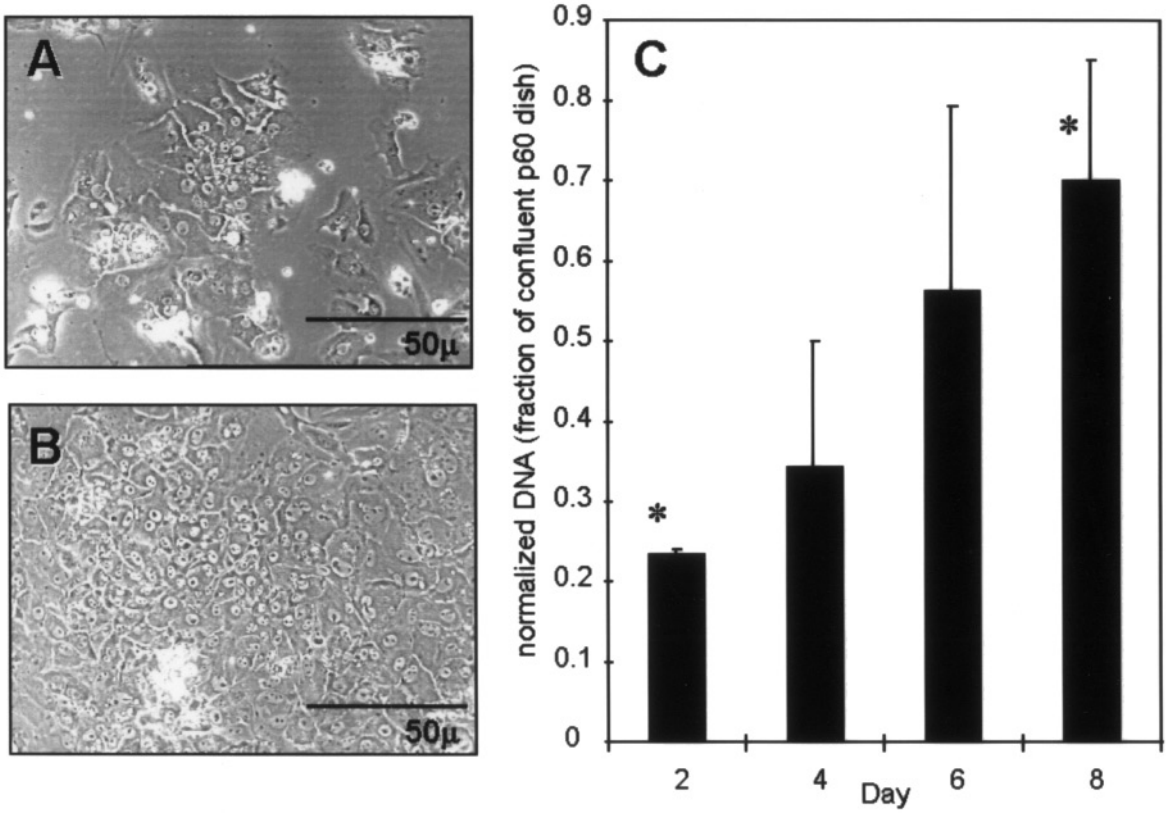

FIG. 6. Porcine hepatocyte morphology on Day 2 (A) and Day 4 (B) demonstrating qualitative increase in apparent cell number. Composite DNA values of OUR experiments are shown in (C), again indicating progressive increase in total cell DNA. Error bars represent standard deviation obtained from quadruplicate daily experiments with triplet DNA measurement, from two porcine hepatocyte isolations, for a total n of 24 per day. Asterisks on (C) indicate statistical significance ($p < 0.05$) of mean difference, as calculated by ANOVA.

operator prone to amplifying minute variations in the source data set (Press *et al.*, 1992b). With optimal low-pass DSP filtering, the consequent OUR curves are representative of the true oxygen consumption rates, without coloration from out-band noise. This allowed for more precise determination of both V_{max} and $K_{0.5}$ values.

The higher initial OUR depicted in Fig. 5 was a pattern exhibited in most of the experiments of this study, as well as our prior publication on this device (Foy *et al.*, 1994). Investigation of polarographic electrode characteristics revealed that the reported PO_2 is a function of temperature, oxygen concentration, and pressure. During the final phases of OUR device assembly, significant mechanical pressure was applied in order to firmly fit the OUR insert within the p60 dish. During this process, the intracavity pressure transiently increased, with a corresponding transient increase in measured oxygen tension. Within approximately 5 min, the electrode restabilized to its calibrated starting level, indicating that cavity pressure had reequilibrated to ambient conditions.

Device Validation

With the above preparative and numerical techniques in place, OUR experiments were performed with rat hepatocytes, to validate system design changes from our previous work. Results of previously reported and current OUR results are presented in Table 1. Day 0 conditions differed from the prior study in that hepatocytes were allowed to attach to the P60 culture dish for a 4-h incubation period prior to measurement. Day 1 Conditions were identical in both studies. Overall, the repeated experiments demonstrated excellent agreement with our original published values.

OUR Measurement of Porcine Hepatocytes

As absolute cell number has a direct impact on the calculation of OUR, a quantitative cell number index was necessary. Figures 6A and 6B illustrate typical culture morphology on postseeding Days 2 and 4, respectively, demonstrating a qualitative increase in cell number. Typically, P60 culture dishes which were only 25% confluent on postseeding Day 1, would reach complete confluence by Day 4. Quantitative DNA assessment following OUR measurements (Fig. 6C) show a progressive increase in DNA fraction until Day 8, at which time an approximate threefold increase in DNA was noted.

OUR measurements taken between postseeding Days 2 and 16 were calculated with and without DNA index normalization (Figs. 7A and 7B). Without DNA normalization, maximal values of 0.45 nM 0_2/s/P60 dish occurred between Days 4 and 8, with rates decreasing to 0.27 by Day 15.

TABLE 1

V_{max} and $K_{0.5}$ of Rat Hepatocytes from our Study Compared to Published Literature Values at Day 0 and Day 1 of Culture

	Day 0		Day 1	
Measurement	Foy *et al.*, 1994	This study	Foy *et al.*, 1994	This study
n	4	6	4	6
V_{max}(nMol/s/10^6 cells)	0.43 ± 0.04	0.35 ± 0.05	0.38 ± 0.12	0.33 ± 0.01
$K_{0.5}$(mm Hg)	2.6 ± 0.5	11.24 ± 0.4	5.6 ± 0.5	4.36 ± 0.13

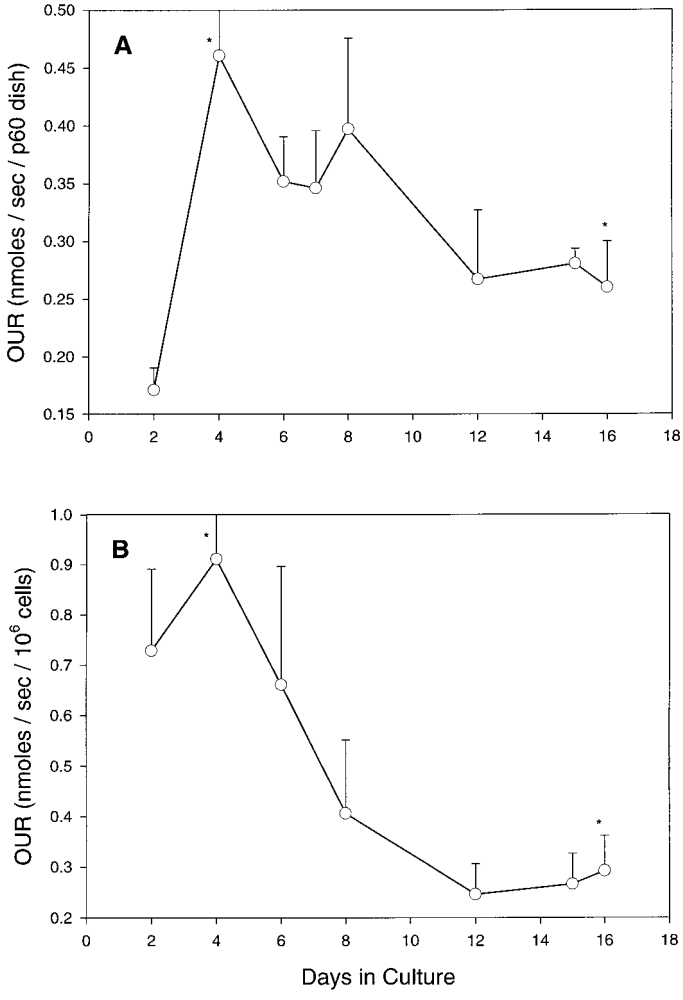

FIG. 7. OUR as a function of days in culture without (A) and with (B) DNA correction to normalize to 1×10^6 cells. Error bars represent standard deviation obtained from quadruplicate daily experiments, from two porcine hepatocyte isolations, for a total n of 12 per day. Asterisks indicate statistical significance ($p < 0.05$) of mean difference, as calculated by ANOVA.

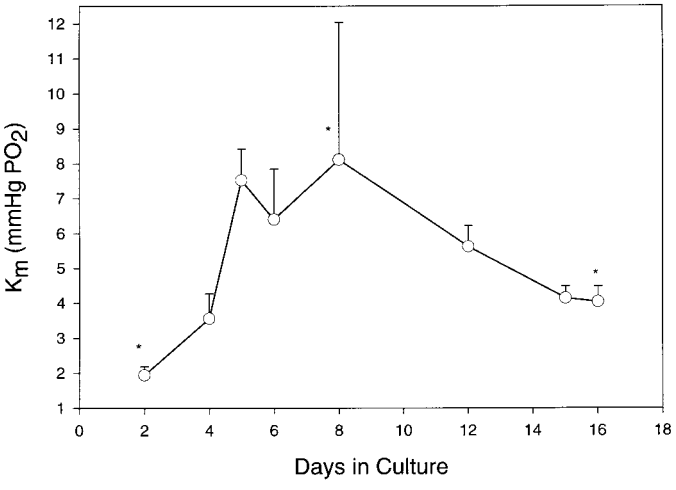

FIG. 8. $K_{0.5}$ values of porcine hepatocytes as a function if days in culture. Results are based upon 38 experiments, from two hepatocyte isolations. Error bars represent standard deviation obtained from quadruplicate daily experiments, from two porcine hepatocyte isolations, for a total n of 12 per day. Asterisks indicate statistical significance ($p < 0.05$) of mean difference, as calculated by ANOVA.

The initial OUR of 0.17 nM 0_2/s/P60 at Day 2 rapidly increased in the following two days. Following DNA normalization of OUR rates, V_{max} was noted to decline from a peak of 0.91 nM O_2/s/1×10^6 cells at Day 4. OUR values decreased from Day 4 to a relative plateau of 0.31 by Day 16.

$K_{0.5}$ values obtained from OUR curves (Fig. 8) an initial increase from 1.9 mm Hg at Day 2 to 7.6 mm Hg at Day 5 of culture. Thereafter, $K_{0.5}$ remained relatively constant for the subsequent 4 days, followed by a steady decline to 4.0 mm Hg by Day 16. DNA normalization was not necessary for the calculation of $K_{0.5}$, as the $\frac{1}{2}$ maximal rate oxygen tension point was not dependent on the absolute OUR.

DISCUSSION

With the anticipated need for approximately 2×10^{10} hepatocytes in a BAL assist device for human support (Gerlach, 1996; Naik *et al.*, 1996; Sakai *et al.*, 1996), it is critical to further characterize the oxygen consumption of porcine hepatocytes which will likely be employed in these devices. We extended our earlier methodology for the measurement of OUR of attached cells to porcine hepatocytes, over a range of oxygen tension which might be encountered in typical bioreactor topologies (Foy *et al.*, 1994). Specifically, numerical analysis enhancements were implemented to allow for accurate and precise assessment of V_{max} and $K_{0.5}$ values, as these data, specifically, dictate design constraints predictive of optimal bioreactor function. With the migration to automated computation methodologies afforded by the DaDISP software package, significant gains in inter-experiment measurement consistency were realized, with perhaps the most salient improvement over our prior work being the capability for accurately measuring oxygen tensions at essentially anoxic levels. Consequently, the accurate measurement of $K_{0.5}$ became somewhat less vexing, as small-scale leakage artifacts no longer dominated the device performance in the sub-5 mm Hg PO_2 region.

The on-line Polarographic oxygen electrode measurement technique employed in this study compares favorably with several alternative techniques reported in the literature. Kyung *et al.* (1994) have reported success with an air-fluid interface indirect technique based on equilibration modeling. However, the ten minute equilibration time yields a slower than real-time measurement capability. Similarly, indirect measurement of oxygen tension by a fluorescent reporter molecule has been repeatedly implemented with varying degrees of success (Benson and Knopp, 1984; Benson *et al.*, 1980; Knopp and Longmuir, 1972). This technique is hampered by inaccuracy arising from difficulties in deriving an absolute oxygen tension baseline reference from rapidly quenching fluorescence signals. Finally, electron paramagnetic resonance (EPR) oximetry has been used successfully to measure OUR (Jiang *et al.*, 1996). Although accurate, EPR oximetry is unsuitable for long-term monitoring because it involves prolonged hepatocyte exposure to India ink and lithium phthalocyanine, compounds with potential cumulative hepatotoxicities.

OUR device oxygen tension vs time raw data for a typical experiment demonstrated a linear decline in oxygen tension until the partial pressure of oxygen approached the $K_{0.5}$ region, typically at tensions between 5 and 15 mm Hg PO_2. Subsequently, oxygen tension decrease would continue at slower rates, with the final asymptote being 0 mm Hg PO_2. This OUR device behavior differed from that reported by Foy *et al.* (1994) who reported final tensions in the range of 1 mm Hg. A probable source for this difference was the use of an outer nitrogen jacket to shield the OUR device from external oxygen ingress, and subsequent quiescent baseline elevation.

Examination of the V_{max} and $K_{0.5}$ data obtained in this study revealed different cellular metabolic states for the initial attachment phase and the subsequent steady-state culture condition. Initial metabolic behavior appears to be dominated by high oxygen consumption and a corresponding low $K_{0.5}$ value. Taken together, these two values represent a cellular metabolic state exquisitely sensitive to rapid hypoxic injury. This results from both the potential for rapid depletion of dissolved oxygen (high V_{max}) and the relatively

narrow oxygen tension range where OUR shifts from maximal to quiescent (dictated by a low $K_{0.5}$). Furthermore, this effect was magnified as these early-culture OUR curves also exhibited a much higher slope in the $K_{0.5}$ transition region as compared to later cultures, further contributing to the propensity for rapid and total depletion of dissolved oxygen. This finding was congruous with results previously reported by Rotem *et al.* (1992), where maximal oxygen consumption rates were seen in recently seeded rat hepatocyte cultures. In his study, OUR was strongly correlated with spreading rate of hepatocytes, suggesting the mechanical process of cell attachment is at least partially responsible for hypermetabolism. Similarly, our non-DNA-corrected data reproduced that reported by Rotem *et al.*, demonstrating a 40% decrease in OUR from the initial period after seeding to stable long-term cultures. Although an alternative explanation for decreased OUR as a function of time in culture may be the preferential growth of mesenchymal cells with relatively low OUR's, we rule out this possibility for the following reasons. First, the late cultures showed polygonal morphology, characteristic of hepatocytes. Second, our *in situ* albumin staining of the initial cell population (data not shown) indicated an initial contamination less than 5%, by counting nonstained cells.

V_{max} and $K_{0.5}$ data obtained from steady-state cultures at Day 10 and beyond differed from earlier cultures. Under these conditions, both the OUR and $K_{0.5}$ were significantly reduced compared to their values in early cultures. This is beneficial from the point of view of designing a bioartificial liver device using porcine hepatocytes because cells are less likely to be exposed to anoxic conditions.

In light of the above time differences in culture behavior, it is desirable when designing optimal BAL bioreactor topologies, to insure that the device oxygenation characteristics will be adequate for all culture periods, as opposed to only steady-state late-culture optimization. As porcine hepatocytes exhibit different OUR-culture age dynamics than previous reported for rat cells, it may be presumed that this difference will extend to other xenogenic hepatocyte candidates, serving as a strong motivation for the rigorous characterization of their OUR characteristics as well. Consequently, failure to correctly characterize new xenogeneic cells might predispose ill-informed BAL designs to hypoxia during high-demand cell-process phases such as spreading and attachment.

Alternative topologies to attachment-based BAL designs include both hollow-fiber and spheroid-microcarrier cell packaging schemes. Nyberg *et al.* (1992b, c) investigated OUR in a hollow-fiber device seeded with hepatocytes suspended in a collagen gel. While rat hepatocyte OUR rates in this topology were relatively consistent over a seven day period, they yielded low values of between 10 and 14 μM/h. This low value led them to hypothesize that oxygen was rate limiting within the central portion of the gels. To answer this question, they performed fluorescence confocal microscopy on gel cross-sections, using a vital stain, and obtained viabilities ranging from 41.9 to 46.3%. Moreover, their analysis of individual optical sections led them to conclude that viability decreased with increasing gel depth, providing strong evidence for mass transfer limitations of oxygen. Concurrently, they concluded that hepatocyte viability was also diminished by the processes of suspension and injection, both being process steps unique to the gel formation methodology. Similarly, Hu *et al.* (1997) has also reported decreased cell viability when the BAL design was changed to hepatocyte spheroids in hollow-fibers. carriers. As the length scale of these structures is comparable to that of Nyberg's cylinders, similar mass transfer limitations can be presumed to be in effect. The observed necrotic zone and decreased viability in these BAL devices provide strong motivation for the continued investigation of direct measurement of OUR for hepatocytes, especially from clinically relevant species.

In summary, we have presented a powerful and robust technique for the accurate measurement of OUR values exhibited by attachment-dependent cells. The combination of on-line and off-line numerical and spectral computational tools allows for both precise signal noise characterization and its subsequent removal, with exceptionally low colorization of resultant data. Our data show that immediately postseeding, porcine hepatocytes exhibit OURs at least twice and $K_{0.5}$ values of one-half that of rat cells. V_{max} values for porcine hepatocytes, encountered after one week postseeding, suggest that the cells evolve from their initial hypermetabolic state, to OUR levels approximately fourfold higher than exhibited by rat hepatocytes. Similarly, steady-state porcine $K_{0.5}$ values are two to three times higher than rat hepatocyte values. These results highlight the potential for xenogeneic variability in OUR characteristics and provide substantial motivation for precise species-specific OUR characterization prior to selection and fabrication of an optimized BAL topology. Finally, in selecting optimal BAL designs, it is clear that the different OUR states of initial and steady-state cultures must be taken into account to assure maximal cell viability for all anticipated metabolic states.

ACKNOWLEDGMENTS

This work was partially supported by grants from Organogenesis, Inc., and The Whitaker Foundation. We are grateful for insightful consultation and technical assistance from Joseph LeDoux, Kyongbum Lee, Ned Jastromb, Christopher Connolly, and Paul Gregory.

REFERENCES

Bader, A., Knop, E., Fruhauf, N., Crome, O., Boker, K., Christians, U., Oldhafer, K., Ringe, B., Pichlmayr, R., and Sewing, K. F. (1995). Reconstruction of liver tissue in vitro: geometry of characteristic flat bed, hollow fiber, and spouted bed bioreactors with reference to the in vivo liver, *Artif. Organs* **19**, 941–950.

Benson, D. M., and Knopp, J. A. (1984). Effect of tissue absorption and microscope optical parameters on the depth of penetration for fluorescence and reflectance measurements of tissue samples, *Photochem. Photobiol.* **39**, 495–502.

Benson, D. M., Knopp, J. A., and Longmuir, I. S. (1980). Intracellular oxygen measurements of mouse liver cells using quantitative fluorescense video microscopy, *Biochem. Biophys. Acta* **591**, 187–197.

Dixit, V. (1994). Development of a bioartificial liver using isolated hepatocytes, *Artif. Organs* **18**, 371–384.

Dunn, J. C. Y., Tompkins, R. G., and Yarmush, M. L. (1991). Long-term in vitro function of adult hepatocytes in a collagen sanwich configuration, *Biotechnol. Prog.* **7**, 237–245.

Elsdale, T., and Bard, J. (1972). Collagen substrata for studies on cell behavior, *J. Cell Biol.* **54**, 626–637.

Foy, B., Rotem, A., Toner, M., Tompkins, R. G., and Yarmush, M. L. (1994). A device to measure the oxygen uptake rates of attached cells: importance in bioartificial organ design, *Cell Transplant.* **3**, 515–527.

Gerlach, J., Kloppel, K., Stoll, P., Vienken, J., and Muller, C. (1990). Gas supply across membranes in bioreactors for hepatocyte culture, *Artif. Organs* **14**, 328–333.

Gerlach, J. C. (1996). Development of a hybrid liver support system: A review, *Int. J. Artif. Organs* **19**, 645–654.

Gerlach, J. C., Encke, J., Hole, O., Muller, C., Ryan, C. J., and Neuhaus, P. (1994). Bioreactor for a larger scale hepatocyte in vitro perfusion, *Transplantation* **58**, 984–988.

Hu, W. S., Friend, J. R., Wu, F. J., Sielaff, T., Peshwa, M. V., Lazar, A., Nyberg, S. L., Remmel, R. P., and Cerra, F. B. (1997). Development of bioartificial liver employing xenogeneic hepatocytes, *Cytotechnology* **23**, 29–38.

Hughes, R. D., and Williams, R. (1996). Use of bioartificial and artificial liver support devices, *Semin. Liver Dis.* **16**, 435–444.

Jauregui, H. O., Chowdhury, N. R., and Chowdhury, J. R. (1996). Use of mammalian liver cells for artificial liver support, *Cell Transplant.* **5**, 353–367.

Jian, J., Nakashima, T., Liu, K. J., Goda, F., Shima, T., and Swartz, H. M. (1996). Measurement of PO_2 in liver using EPR oximetry, *J. Appl. Physiol.* **80**, 552–558.

Knopp, J. A., and Longmuir, I. S. (1972). Intracellular measurement of oxygen by quenching of fluorescence of pyrenebutyric acid, *Biochim. Biophys. Acta* **279**, 393–397.

Krantz, S. J. (1991). Fast Fourier Transforms, *in* "Studies in Advanced Mathematics" (J. S. Wallser, Ed.), 1st ed., CRC Press, Boca Raton, Fl.

Kyung, Y., Peshwa, M. V., Gryte, D. M., and Hu, W. (1994). High density culture of mammalian cell with dynamic perfusion based on on-line oxygen uptake rate measurements, *Cytotechnology* **14**, 183–190.

McGuire, B. M., Sielagg, T. D., Nyberg, S. L., Hu, M. Y., Cerra, F. B., and Bloomer, J. R. (1995). Review of support systems used in the management of fulminant hepatic failure, *Dig. Dis.* **13**, 379–388.

Naik, S., Trenkler, D., Santangini, H., Pan, J., and Jauregui, H. O. (1996). Isolation and culture of porcine hepatocytes for artificial liver support, *Cell Transplant.* **5**, 107–115.

Nyberg, S. L., Shatford, R. A., Hu, W. S., Payne, W. D., and Cerra, F. B. (1992a). Hepatocyte culture systems for artificial liver support: implications for critical care medecine (bioartificial liver support), *Crit. Care Led.* **20**, 1157–1168.

Nyberg, S. L., Shatford, R. A., Hu, W. S., Payne, W. D., and Cerra, F. B. (1992b). Primary culture of rat hepatocytes entrapped in cylindrical collagen gels: An in vitro system with application to the bioartificial liver. Rat hepatocytes cultured in cylindrical collagen gels, *Cytotechnology* **10**, 205–215.

Nyberg, S. L., Shatford, R. A., Peshwa, M. V., White, J. G., Cerra, F. B., and Hu, W.-S. (1992c). Evaluation of Hepatocyste-entrapment hollow fiber bioreactor: A potential bioartificial liver, *Biotech. Bioeng.* **41**, 194–203.

Nyberg, S. L., Remmel, R. P., Mann, H. J., Peshwa, M. V., Hu, W. S., and Cerra, F. B. (1994). Primary hepatocytes outpeform Hep G2 cells as the source of biotransformation functions in a bioartificial liver, *Ann. Surg.* **220**, 59–67.

Press, W. H., Teukolsky, S. A., Vetterling, W. T., and Flannery, B. P. (1992a). *in* "Numerical Recipes in C: the art of scientific computing," 2nd ed., pp. 650–655, Cambridge Univ. Press, Cambridge.

Press, W. H., Teukolsky, S. A., Vetterling, W. T., and Flannery, B. P. (1992b). *in* "Numerical Recipes in C: The art of scientific computing," 2nd ed., pp. 186–189, Cambridge Univ. Press, Cambridge.

Rottem, A., Toner, M., Tompkins, R. G., and Yarmush, M. L. (1992). Oxygen uptake rates in cultured rat hepatocytes, *Biotech. Bioeng.* **40**, 1286–1291.

Sakai, Y., Naruse, K., Nagashima, I., Muto, T., and Suzuki, M. (1996). Large-scale preparation and function of porcine hepatocytes spheroids, *Int. J. Artif. Organs* **19**, 294–301.

Shatford, R. A., Nyberg, S. L., Meier, S. J., White, J. G., Payne, W. D., Hu, W. S., and Cerra, F. B. (1996). Hepatocyte function in a hollow fiber bioreactor: a potential bioartificial liver, *J. Surg. Res.* **53**, 549–557.

Sielaff, T. D., Nyberg, S. L., Rollins, M. D., Hu, M. Y., Amiot, B., Lee, A., Wu, F. J., Hu, W. S., and Cerra, F. B. (1997). Characterization of the three-compartment gel-entrapment porcine hepatocytes bioartificial liver, *Cell Biol. Toxicol.* **13**, 357–364.

Starlinger, H., and Lubbers, D. W. (1972). Methodical studies on the polarographic measurement of respiration and critical oxygen pressure in mitochondria and isolated cells with membrane-covered platinum electrodes, *Pflugers Arch.* **337**, 19–28.

Steen, R. G., MacDonald, C. G., Weaver, A. L., and Pitt, A. M. (1993). Rapid fluorescence quantitation of plasmid miniprep DNA, *Biotechniques* **15**, 932–933.

Stefanovich, P., Matthew, H. W. T., Toner, M., Tompkins, R. G., and Yarmush, M. L. (1996). Extracorpoeal plasma perfusion of cultured hepatocytes: effect of intermittent perfusion on hepatocytes function and morphology, *J. Surg. Res.* **66**, 57–63.

Vanderkooi, J. M., Erecinska, M., and Silver, I. A. (1991). Oxygen in mammalian tissue: methods of measurement and affinities of various reactions, *Amer. J. Physiol.* **260**, 1131–1150.

Yarmush, M. L., Toner, M., Dunn, J. C., Rotem, A., Hubel, A., and Tompkins, R. G. (1992). Hepatic tissue engineering. Development of critical technologies, *Ann. N.Y. Acad. Sci.* **665**, 238–252.